

PALACKÝ UNIVERSITY OLOMOUC  
FACULTY OF SCIENCE  
JOINT LABORATORY OF OPTICS

**BACHELOR THESIS**

Calibration and monitoring of astroparticle  
telescopes



Author: **Daniel Staník**  
Study program: B0533A110007 Applied Physics  
Field of study: 1702R001 Applied Physics (AFYZ)  
Form of study: Full-time  
Supervisor: Ing. Ladislav Chytka, Ph.D.  
Deadline: April 2022

## **DECLARATION**

I hereby declare that I elaborated this bachelor thesis independently under the supervision of Ing. Ladislav Chytka, Ph.D., using only information sources referred in the Literature chapter.

In Olomouc December 17, 2021

.....

Daniel Staník

# Bibliographical identification

Autor's first name and surname	Daniel Staník
Title	Calibration and monitoring of astroparticle telescopes
Type of thesis	Bachelor
Department	Joint Laboratory of Optics
Supervisor	Ing. Ladislav Chytka, Ph.D.
The year of presentation	2022
Abstract	<p>Lorem ipsum dolor sit amet, consectetur adipiscing elit. Curabitur et lectus sit amet lectus vestibulum dignissim. Cras sit amet enim vitae mi elementum blandit eget nec tortor. Curabitur eget eros vitae arcu luctus varius commodo vel mauris. Nam elementum convallis pretium. Nunc dignissim pulvinar urna, nec blandit ante fringilla at. Ut et magna purus, vel pellentesque massa. In tortor nisi, faucibus condimentum cursus ut, sollicitudin quis leo. Ut at purus nec arcu accumsan tincidunt id id massa. Nam id vehicula mi.</p> <p>keyword 1, keyword 2, ...</p>
Keywords	
Number of pages	xx
Number of appendices	x
Language	english

# Bibliografická identifikace

Jméno a příjmení autora	Daniel Staník
Název práce	Kalibrace a monitorování astročásticových teleskopů
Typ práce	Bakalářská
Pracoviště	Společná Laboratoř Optiky
Vedoucí práce	Ing. Ladislav Chytka, Ph.D.
Rok obhajoby práce	2022
Abstrakt	<p>Lorem ipsum dolor sit amet, consectetur adipisciing elit. Curabitur et lectus sit amet lectus vestibulum dignissim. Cras sit amet enim vi- tae mi elementum blandit eget nec tortor. Cur- abitur eget eros vitae arcu luctus varius com- modo vel mauris. Nam elementum convallis pretium. Nunc dignissim pulvinar urna, nec blandit ante fringilla at. Ut et magna purus, vel pellentesque massa. In tortor nisi, faucibus condimentum cursus ut, sollicitudin quis leo. Ut at purus nec arcu accumsan tincidunt id id massa. Nam id vehicula mi.</p>
Klíčová slova	klíčové slovo 1, klíčové slovo 2, ...
Počet stran	xx
Počet příloh	x
Jazyk	anglický

# Contents

<b>Introduction</b>	<b>7</b>
<b>1 Astroparticle detection</b>	<b>8</b>
1.1 Cosmic rays and particles . . . . .	8
1.1.1 Primary cosmic rays . . . . .	8
1.1.2 Secondary cosmic rays . . . . .	9
1.2 Ultra-high energy cosmic rays (UHECRs) . . . . .	9
1.3 UHECRs detection techniques . . . . .	10
1.3.1 Air fluorescence . . . . .	10
1.3.2 Surface particle detection . . . . .	11
1.3.3 Cherenkov light detection . . . . .	11
1.3.4 Hybrid detection . . . . .	11
1.4 UHECRs observatories . . . . .	11
1.4.1 Pierre Auger observatory . . . . .	11
1.4.2 Telescope array project . . . . .	11
<b>2 FAST telescope</b>	<b>12</b>
2.1 FAST detection and operation scheme . . . . .	12
2.2 Protection hut . . . . .	12
2.3 Remote control and monitoring . . . . .	13
2.4 . . . . .	13
<b>3 Calibration of astroparticle detectors</b>	<b>14</b>
3.1 Absolute calibration . . . . .	14
3.2 Relative calibration . . . . .	14
3.3 FAST calibration . . . . .	14
3.3.1 Flasher . . . . .	14
3.3.2 YAP pulser . . . . .	14
3.3.3 Homogenous light source . . . . .	14
<b>4 Instrumentalization and measurement preparation</b>	<b>15</b>
4.1 Integration sphere . . . . .	15
4.2 Photomultiplier tube . . . . .	16
4.2.1 Operating principle . . . . .	16
4.2.2 Dark current . . . . .	19
4.2.3 Timing and response . . . . .	19
4.2.4 Operating life and degradation . . . . .	20
4.2.5 FAST's PMTs . . . . .	20
4.2.6 Calibration . . . . .	20
4.3 Silicon PM . . . . .	20

4.4	Hardware for experiment control . . . . .	20
4.4.1	Raspberry Pi . . . . .	20
4.4.2	STM32 based microcontrollers . . . . .	20
4.4.3	USB oscilloscope . . . . .	20
4.4.4	PM16 optical Power meter . . . . .	20
4.5	Sensors and other electronics components . . . . .	20
4.5.1	MPU6050 . . . . .	20
4.5.2	servo motors . . . . .	20
4.5.3	Dallas DS18B20 thermometer . . . . .	20
<b>5</b>	<b>Calibration UV optical source</b>	<b>21</b>
5.1	Karlsruhe UV source . . . . .	21
5.2	Testing and measurement of UV source . . . . .	22
5.2.1	Measuring apparatus . . . . .	22
5.2.2	Data acquisition and analysis . . . . .	24
5.2.3	Results . . . . .	26
5.3	UV LED diode aging . . . . .	31
5.4	Optical feedback - potential fix . . . . .	31
5.4.1	Detection photodiode . . . . .	31
5.5	Modified UV source for drone mounting . . . . .	34
<b>6</b>	<b>Monitoring system</b>	<b>35</b>
6.1	Monitoring of multiple FAST telescopes . . . . .	35
6.2	Control units and sensors . . . . .	35
6.3	Software system . . . . .	36
<b>7</b>	<b>FAST Calibration data analysis</b>	<b>38</b>
7.1	Photomultiplier relative calibration . . . . .	38
7.2	. . . . .	38
7.3	. . . . .	38
<b>Conclusion</b>		<b>39</b>

# Introduction

Lorem ipsum dolor sit amet, consectetur adipiscing elit. Curabitur et lectus sit amet lectus vestibulum dignissim. Cras sit amet enim vitae mi elementum blandit eget nec tortor. Curabitur eget eros vitae arcu luctus varius commodo vel mauris. Nam elementum convallis pretium. Nunc dignissim pulvinar urna, nec blandit ante fringilla at. Ut et magna purus, vel pellentesque massa. In tortor nisi, faucibus condimentum cursus ut, sollicitudin quis leo. Ut at purus nec arcu accumsan tincidunt id id massa. Nam id vehicula mi.

<http://exfyz.upol.cz/didaktika/>

# Chapter 1

## Astroparticle detection

More than 100 years have passed since Victor Franz Hess first encountered cosmic radiation. Since those times the techniques and methods of detection have been strongly improved. We have moved up from elevating electroscopes by balloons to observe growing electric charge to specialized techniques, which allows us to measure particles' energies, trajectories, etc.

### 1.1 Cosmic rays and particles

Cosmic rays is a term for radiation and energetic particles striking earth atmosphere with an origin in outer space sources (neutron stars, supernovas, black holes, etc). There are two types of cosmic rays - primary and secondary. Primary cosmic rays are the original cosmic particles, which strike the Earth's atmosphere. Secondary cosmic rays (also referred as showers) are particles, which have origin in particle interaction between primary cosmic rays and the atmosphere.



Figure 1.1: Illustration of cosmic rays striking Earth's atmosphere (credit: A. Chantelauze, S. Staffi, L. Bret) [8].

#### 1.1.1 Primary cosmic rays

Primary cosmic rays consist of protons (95%), helium nuclei (4%), electrons and other heavy nuclei (up to iron). However, only the highly energetic rays make their way to the atmosphere. The Earth's magnetic field affects their trajectories and prevents the low-energetic (less than 100 MeV) particles from arriving to the atmosphere [6].

Part of primary cosmic rays are also Ultra-high energy cosmic rays (UHECRs), which we refer in the next chapter.

Neutrinos are also a part of cosmic radiation, but their interaction with matter is very rare, so they are very hard to detect. The special underwater detectors are developed to detect some of them.

### 1.1.2 Secondary cosmic rays

Secondary cosmic rays are created by interaction of high-energetic particles of primary component with air nuclei, such as nitrogen. They consist of low-energetic and high-energetic muons, gamma photons, electrons and positrons. Most of muons travel up to the earth's surface although their half-life is only about 2.2 microseconds before they decay into electrons and neutrinos. Due to their high relativistic speeds, their half-life is increased for external observers.

## 1.2 Ultra-high energy cosmic rays (UHECRs)

UHECRs are particles with energies from  $10^{18}$  to  $10^{20}$  eV, which is much more than particles created on Cern's Large hadron colider (LHC) with energies about  $10^{13}$ . Due to their high energies, the trajectory remains nearly unchanged by space magnetic fields [9].

UHECRs' origin is yet unknown, but it is supposed and experimentally proved that they come from outside of the Milky Way. Some theoretical physicists expect, that the one possible source of UHECRs acceleration are the starburst galaxies. One of UHECR possible particle is proton.

In many particle physics experiments, some form of calorimeter is used to determine the particles' energy and direction. In case of UHECRs, the air molecules of atmosphere have the function of calorimeter. When UHECR interacts with atmospheric nuclei, the cascade of particles is induced. This cascade concists of three main components: electromagnetic, hadronic and muonic. It is also referred to as extensive air shower (EAS).

In case of ultra-high energy proton striking an air molecule, kaons, baryons, nuclear fragments and mostly pions are created. Together, they are referred as hadronic component. The pions with short lifetime decay into electromagnetic sub-shower. The behaviour of pions with longer lifetime is energy-dependent. At higher energies they reinteract with atmospheric nuclei and feed hadronic and electromagnetic component. At lower energies they decay into muonic component with muonic neutrinos. The muons with short lifetime decay into electrons and positrons with neutrinos, which join the electromagnetic cascade, while the others reach the Earth's surface carrying the energy, which we are unable to detect. The UHECR's cascade scheme is shown in Fig. 1.2.

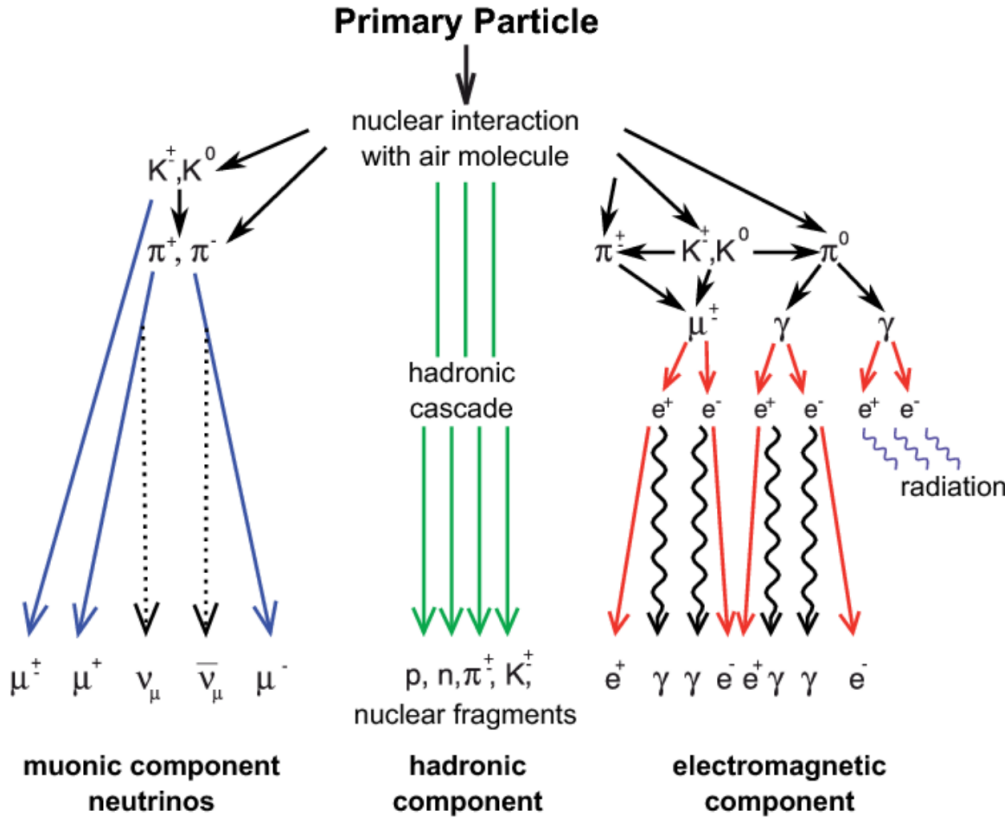


Figure 1.2: UHECR's cascade, taken from [2].

The electromagnetic cascade consisting of electron, positrons, gama photons carries the most of UHECR's original energy. With increasing depth, the cascade develops by decaying the photons into electron and positron pairs, which again emit photons and this process repeats. The cascade develops until the the energy treshold is reached, where the ionization is higher than the radiation losses. [1].

One of the main parameters of electromagnetic cascade is  $X_{max}$  - the point along the shower axis, where is the maximum of deposited energy.

## 1.3 UHECRs detection techniques

Nowadays there are three main proven techniques to detect UHERCs - air fluorescence, surface particle detection and Cherenkov light detection.

### 1.3.1 Air fluorescence

The electrons and positrons from electromagnetic cascade excite nitrogen molecules, which then deexcite and emit fluorescence light in UV spectre with two main wavelengths 337 and 357 nm. The intensity of this light is directly proportional to the calorimetric energy of the shower.

However, the intensity of this light is very low, and thus the measurements must be done in dark nights with no light smog. Even a low intensity of external sources could led to detection of false events or worse - the unwanted light could damage the very sensitive equipment.

The detection equipment are mostly the superreflective UV mirrors which focus part of the UV shower into the PMT or into the camera based on PMTs. It it necessary to

have atmospheric monitoring system (temperature, humidity, pressure etc.) along with the detection part, because the fluorescence is highly dependent on these conditions.

The main advantage of fluorescence detection is the fact, that by measuring and integrating the light profile we are able to calculate the total calorimetric energy. However, corrections

The FAST telescope, on which we focus in this thesis, is considered to be a fluorescence telescope.

### **1.3.2 Surface particle detection**

Surface particle detection is a method, which is based on detecting individual particles from EAS. There are two proven surface techniques to detect EAS - by scintillators or water Cherenkov detectors. To detect the EAS full geometric distribution, the huge surface needs to be covered by surface detectors.

Compared to fluorescence detection method, the surface detectors don't require the dark night and any light exposure is not a threat for them.

### **1.3.3 Cherenkov light detection**

### **1.3.4 Hybrid detection**

## **1.4 UHECRs observatories**

### **1.4.1 Pierre Auger observatory**

### **1.4.2 Telescope array project**

# Chapter 2

## FAST telescope

The Fluorescence detector Array of Single-pixel Telescopes (FAST) is an international project of fluorescence telescope sensitive to UHECRs.

Until today there are four prototypes in active service. Three of them are situated in Black Rock Mesa site of the Telescope Array experiment in central Utah and one in Argentina near Pierre Auger Observatory.

The main goal of FAST project is to develop a cheap fluorescence telescope, which could be used in future to cover the wide surface area. This new oncoming fluorescence telescope array should be able to fully reconstruct the geometry of UHECRs induced UV shower by combining the information from telescopes, which has encountered an event at the same time.

### 2.1 FAST detection and operation scheme

Main detection part of telescope consists of superreflective UV mirrors and photomultipliers.

### 2.2 Protection hut

The entire telescope along with monitoring systems and other instruments is situated in a hut with remote shutter, where it is protected from negative metrological phenomena, such as rain or fast wind, but also from dust and aerosols. Exposure of mirrors to any of this phenomena could lead to reduction of theirs reflectivity. It is also necessary to monitor and protect PMTs from unwanted light sources. Even a low-intensity sources could decrease PMT's service life.



Figure 2.1: FAST telescope's hut in Argentina.

## 2.3 Remote control and monitoring

In case of Argentina prototype, the telescope's systems are connected to Pierre Auger network and through it, the telescope could be controlled and monitored over the internet.

Testing measurements, sometimes referred as shifts, are performed in the night. Their main purpose is to acquire data, which could be later analyzed and compared with data from Los Leones part of Pierre Auger, which has the similar FoV as Argentine FAST. The testing measurements require an operator to look after the telescope systems. An operator's duty is to power on and off the DAQ, PMTs' voltage sources, perform calibration, open and close the shutter and mainly check for failures and negative phenomena. To do that, operator could access webcam (2.2), meteostation with thermometers, humidity, wind and light sensors and the Allsky camera (2.3).



Figure 2.2: FAST telescope with closed shutter from webcam.



Figure 2.3: View from Allsky camera installed atop the hut. It gives the information of sky quality by comparing visible stars with theoretical star map.

## 2.4

# **Chapter 3**

## **Calibration of astroparticle detectors**

Calibration is a process, which we perform to obtain relationships between measured values by tested device and values given by used ethalon. These relationships may be specified by calibration constants, functions or by other mathematical relations. The tested devices could be also calibrated relatively to each other.

In case of astroparticle detection, we mostly need to , ,

### **3.1 Absolute calibration**

### **3.2 Relative calibration**

### **3.3 FAST calibration**

FAST telescope calibration techniques are yet under development. It is necessary to calibrate PMTs both in absolute and relative way, but also the entire telescope as optoelectronical system with mirrors and PMTs.

#### **3.3.1 Flasher**

As was mentioned before, the FAST telescope is equipped with UV LED flasher, which is used to generate light pulses. Calibration by flasher is performed during every shift - two times at the beginning and two times at the end. One time with opened shutter and one time with closed shutter.

#### **3.3.2 YAP pulser**

#### **3.3.3 Homogenous light source**

There is

# Chapter 4

## Instrumentalization and measurement preparation

To perform all of necessary measurements we need to use various types of optical and electronical equipment.

### 4.1 Integration sphere

The Integration sphere (IS) is a special optical equipment, which can be used either as extended uniform light source (EULS) or with spectrometer in determining the material reflectance. In our experiments we use general purpose Labsphere (Fig. 4.1).



Figure 4.1: General purpose Labsphere.

The IS inner surface consist of white optical diffusive material ( $\text{BaSO}_4$  and Poly-tetrafluoroethylene). The IS also contains several circular apertures, which are called

input/output ports. They can be used to mount detectors or optical sources or left free to let light flux enter or exit IS.

The inner surface is part where light integration happens. The effect which takes place here is known as Lambertian scattering. After one spot of inner surface is hit by a ray, the energy should be uniformly radially distributed. In output port this produces a homogenous light source. The homogeneity decreases with increasing number and sizes of input/output ports.

Using optical source with IS requires baffle to prevent source's light flux or its part to exit IS without integration.

More deeper explanation of IS working principles and characterization of optical properties of the identical IS, which we use, can be found in [4].

For our purposes, in case of FAST calibration, we use IS as EULS in UV spectre. In case of testing optical calibration source, we don't even care about homogeneity. The reason why we use IS in this case is that it focuses the optical power of the source into output ports, where our detectors are mounted, and blocks any other external light source, which could affect our detectors.

## 4.2 Photomultiplier tube

Photomultiplier tube (PMT) is considered to be a high voltage optoelectronic part. It allows us to measure very low intensity optical signals. PMT is also characterized by high amplification, low noise and stability. It has many variants of usage. It can be used either as detector of optical signal (pulse or continual) for chosen wavelength or as a radiation detector. We can construct a counter or a multichannel analyzer by mounting an appropriate scintillator on the window of the PMT. The general theory of PMTs is described in more detail in [5, 7].

### 4.2.1 Operating principle

PMT consists of 6 main elements, which can be seen on scheme 4.2.



Figure 4.2: Photomultiplier tube scheme.



Figure 4.3: XP2262 PMT used for our measurements.

The input photon with sufficient energy, which strikes the PMT's photocathode, excites photocathode's electron. This electron then follows electrostatic field to the first dynode of the electron multiplier, where it induces secondary emission of more electrons. These electrons are then attracted by the next dynode, where the emission process repeats. After few times of multiplying electron number over dynodes, the electrons are then collected by the anode, which is situated on the end of the electron multiplier. The anode output current is then converted to voltage signal by appropriate load resistor or by operational amplifier current-to-voltage circuit.

As all other laboratory instruments, which are based on accelerating electrons, such as electron microscopes, the photomultiplier's main parts must be kept in vacuum. To maintain vacuum, the photomultiplier is surrounded by special glass envelope. To avoid mechanical damage of the glass envelope, the entire photomultiplier is situated in a plastic tube.

One of the basic adjustable characteristic of PMT is its gain. The gain is defined as:

$$G = \frac{I_a}{I_p}, \quad (4.1)$$

where  $I_a$  is the anode current and  $I_p$  is the input photocurrent from the photocathode.

In case of ideal, noiseless PMT, we can adjust gain by varying the supply voltage. By varying supply voltage we can adjust gain according to an equation:

$$\frac{G_2}{G_1} = \left(\frac{V_2}{V_1}\right)^{\alpha N}, \quad (4.2)$$

where  $G_2$  and  $G_1$  are gains at supply voltages  $V_2$  and  $V_1$ .  $\alpha$  is coefficient given by dynode material and  $N$  is the number of dynodes.

Other effects, such as temperature, may also vary PMT's gain, and it is necessary to keep them on constant value or measure them and involve them in the final evaluation of data.

For proper functionality of the PMT, the charge and current linearity should be considered. Charge linearity is the ratio of the number of incident photons to the number of electrons collected at the anode. Current linearity express the proportionality between incident light flux and anode current. Ideal PMT is always linear, but the real PMT may vary from linearity due to drifts, space charges, instability of voltage divider etc. These effect can lead up to saturation of the PMT. In saturation, increasing the input light flux leaves the anode current mostly unchanged.

## Window

The photocathode is superimposed by glass window, whose main purpose is to admit light of certain wavelengths. Glass materials are characterized by the spectral sensitivity to wavelengths. For transparency in UV spectre, it is advised to use borosilicate or fused silica glasses.

## Photocathode

The photocathode is the only light-sensitive part of PMT. It transfers the light flux into the electric current.

One of its main parameters is quantum efficiency. It is referred as ratio of emitted photoelectrons to the number of incident photons expressed as a percentage. It is generally less than 35 %. For measurement, the more practical parameter is cathode radiant sensitivity. It is the ratio of photocathode current to an incident light power, which is expressed in mA/W.

Photocathode material must be sensitive to certain wavelengths, which we want to detect with the PMT, and must have sufficient quantum efficiency. Preferred materials are usually alkali antimonides.

## Electron multiplier

The electron multiplier consists of dynodes and one anode. Dynodes are electrodes, which produce more electrons through secondary emission. To maintain electrostatic field between dynodes, each of dynodes is held on different potential. This is achieved by using the voltage divider. Every resistor in the divider sets the potential of one diode according to its resistivity.

All of the photoelectrons emitted by photocathode should be ideally collected by the first dynode. However, many of them could be diverted from their path to anode due to various effects. The parameter, which characterizes this, is the collection efficiency. The Collection efficiency is a probability that photoelectron will strike area of the first dynode.

There are few types of dynodes arrangements. On the fig. 4.2 is the classic linear-focusing multiplier.

## Voltage divider and voltage adjustment

Voltage divider could be a simple resistor serial network, which divide high input voltage between the dynodes.

It is necessary to consider, that the multiplier current density increases in direction to the anode, so it tends to lessen the voltage between last dynode and anode. This phenomena can shake the potential levels across the entire multiplier. One way to reduce the impact on PMT's behaviour is to choose the proper resistor values of the divider.

The resistor values could be same for all the dynodes, but for some applications it is better to have progressive voltage distribution, which increases from cathode to anode, or intermediate distribution with highest values on the beginning of the multiplier.

In some applications, where high anode current peaks are expected, the divider can be filled with reservoir capacitors, which prevent the temporary charge exhaustion of the dynodes. In pulse mode, the unwanted oscillations on dynodes may occur, in that case, it is desirable to connect additional damping resistor to the divider.

Voltage supply should be stable during the PMT's operation. As was mentioned before, the PMT's gain is voltage dependent. To adjust sufficient gain, high voltage (thousands of volts) needs to be applied between photocathode and anode. The high voltage needs to be ramped on required level gradually to avoid negative consequences of transition and dark current effects, which can decrease the operating life of PMT. The same truth is for shutting down the PMT.

The high voltage could be applied to the PMT in negative or positive polarity. In case of positive polarity, the cathode is held at ground and anode on +HV. In case of negative polarity, the cathode is held at -HV and anode at ground.

#### 4.2.2 Dark current

Dark current is anode current produced by photomultiplier in total darkness. It is considered to be a part of unwanted noise, causes errors in measurements and limits the detectivity of PMT. Dark current has origin in Ohmical leakage, thermionic and field emission or in radioactivity. Ohmical leakage is major part of dark current at low gain. With the increasing gain the thermionic emission prevails. At high gains the field emission becomes the major part.

##### Ohmical leakage

Insufficient insulation of electrodes, dynodes and all other parts which are under high voltage may lead to surface current over glass and tube. Dirt and humidity are in most cases the reason of Ohmical leakage.

##### Thermionic emission

Temperature causes emission of photocathode's electrons, which are at medium gains the major part of dark current. Due to this effect, some PMTs may need to be cooled during operation.

##### Field emission

At high gains the electrostatic field is so strong that it can rip the electrons out of the electrodes and accelerate them onto other surfaces, where they cause secondary emission. Field emission rapidly increases with supply voltage. In some literature it is also referred as cold emission.

##### Radioactivity

The radioactivity of PMT's components depends only on the material composition. In some applications, such as astroparticle detection, it is necessary to decrease radiation as possible. In astroparticle detection the radioactivity could be a source of false events. Only way to prevent this is to use materials with a very low concentration of radioactive isotopes.

#### 4.2.3 Timing and response

Differences of photoelectrons' trajectories from the cathode to the first dynode lead into time distortion of signal. For example if we were able to produce delta-function pulse, the PMT would detect pulse with some response width time  $t_w$ . With respect

to differences in electron trajectories and arrival times, the PMTs are divided into 3 types:

1. **Very-fast tubes** - photoelectrons arrive simultaneously, low collection efficiency.
2. **Fast tubes** - compromise between timing performance and collection efficiency
3. **General-purpose tubes** - simple optoelectronics, good collection efficiency, low timing performance

#### **4.2.4 Operating life and degradation**

The operating life of PMT is defined as the time required for anode sensitivity to be halved. If we neglect the outside effects, the operating life mainly depends on anode current. Degradation processes start to show themselves at currents higher than  $10 \mu\text{A}$ . Aging is accompanied by increasing or decreasing gain at stable voltage. Operating life of PMT is measured in thousands of operating hours.

By exposing PMT to bad conditions, such as humidity, mechanical stress, high temperatures or the high-intensity light, the PMT's operating life could be shorten much faster.

#### **4.2.5 FAST's PMTs**

#### **4.2.6 Calibration**

### **4.3 Silicon PM**

### **4.4 Hardware for experiment control**

#### **4.4.1 Raspberry Pi**

#### **4.4.2 STM32 based microcontrollers**

#### **4.4.3 USB oscilloscope**

#### **4.4.4 PM16 optical Power meter**

### **4.5 Sensors and other electronics components**

#### **4.5.1 MPU6050**

#### **4.5.2 servo motors**

#### **4.5.3 Dallas DS18B20 thermometer**

# Chapter 5

## Calibration UV optical source

Blah blah we need it.

### 5.1 Karlsruhe UV source

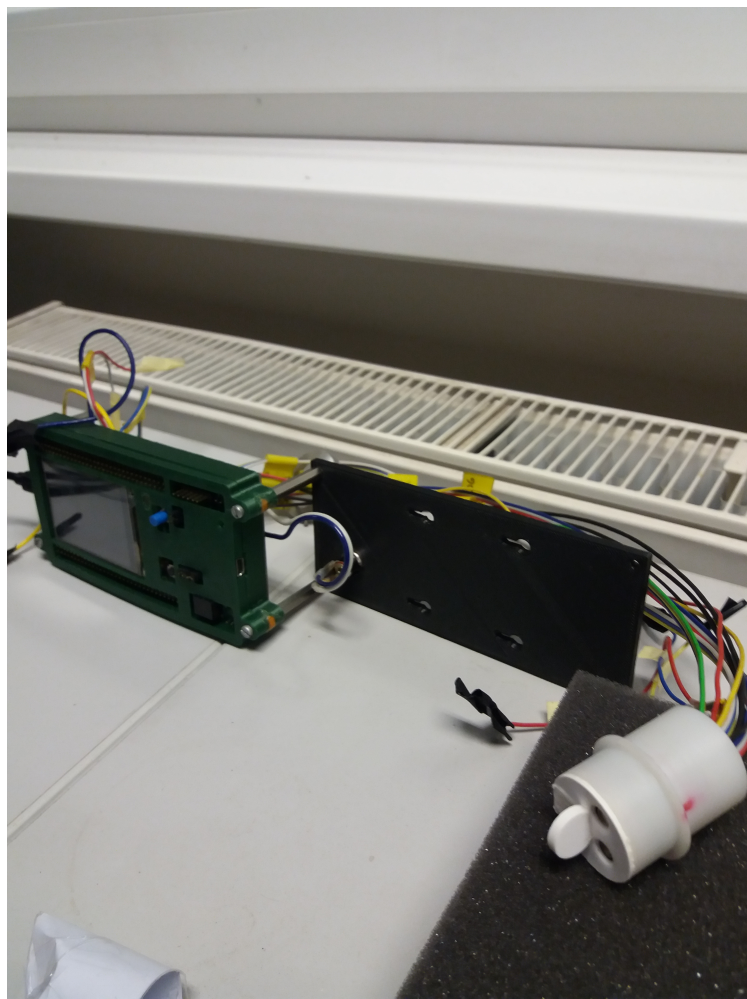


Figure 5.1: UV source constructed by Vladimír Urbášek from SLO according to KIT's template.

Our main task was to test this UV source's longtime stability and develop possible fixes and upgrades.

## 5.2 Testing and measurement of UV source

For calibration UV source, the longtime stability of optical power and pulse geometry is very important. Because there were no specialized apparatus for this measurement, we had to built and program one by ourselves. For these measurements, we use UV source with LED current  $I_d = 2.5$  mA, 50% duty cycle and frequency  $f = 50$  kHz.

### 5.2.1 Measuring apparatus

For measuring the optical power we use PM16 power meter (PM) and for determining the pulse geometry we use XP2262 PMT with signal output connected to 2-channel PicoScope 2205A MSO usb oscilloscope. XP2262 PMT is held on  $U \approx -680$  V by HV voltage source. The PMT's gain may drift over time, but we use PMT mainly for geometry analysis and measurement of absolute optical power is left to PM16.

We also use DS18B20 thermometer for PMT temperature monitoring and keysight 34461a multimeter for checking voltages.

The PMT, power meter and the optical head of UV source are mounted in the IS's ports. The IS stops the unwanted external light and distributes the optical power to PMT and power meter.

The entire apparatus is driven by Raspberry Pi (RPi). The RPi takes care of data acquisition and could be used to set the parameters of the UV source. It could be easily accessed over internet for data download or for user to control the experiment.

Oscilloscope was programmed in C language according to its programmer's manual [10]. It is capable of 2ns sampling which is enough to capture rising edges of the pulses. The RPi sets basic parameters (DC coupling, range etc.) and then activates oscilloscope's trigger (rising edge). After sampling, RPi receives all samples from oscilloscope's memory.

The multimeter is controlled by VISA commands using python USBTMC library. For thermometer we use RPi's 1-Wire.

Main component (IS,PW, PMT with HV source, UV source) are situated in protection box to prevent unwanted manipulations and touching the HV parts. The apparatus could be seen on fig. 5.2 and 5.3.

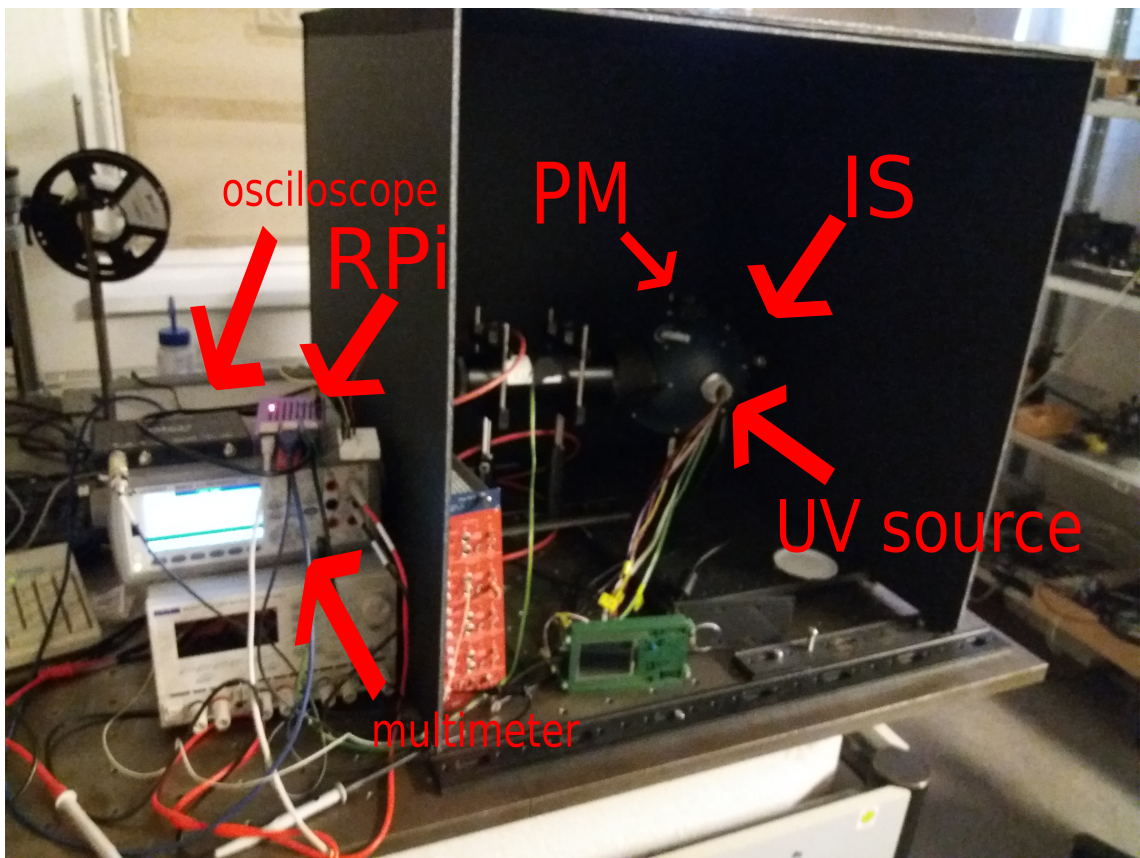


Figure 5.2: Measuring apparatus.

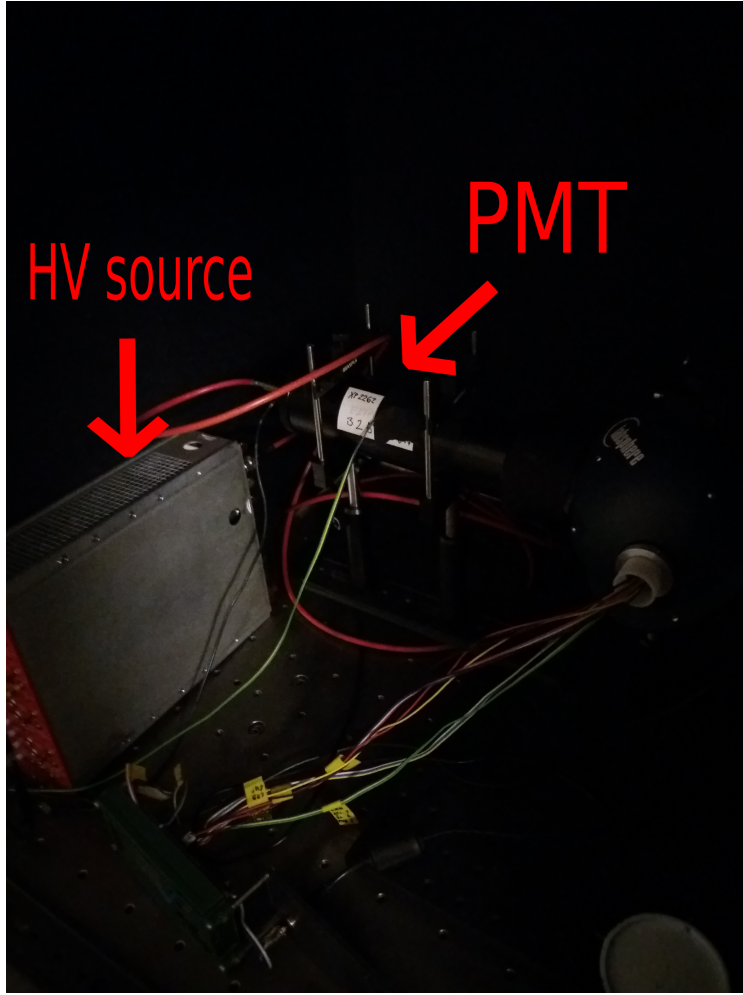


Figure 5.3: PMT mounting and HV source.

### 5.2.2 Data acquisition and analysis

All the data are taken in specified interval (15 or 30 minutes). Two files are produced - oscilloscope waveform file and a file with 30 samples of power meter, multimeter and a thermometer readings. From these 30 samples we calculate average and error. Most of data analysis we perform is done by C/C++ Root framework.

The data from oscilloscope contains the square pulses with noise (fig. 5.4). From them we need to extract the information of pulses height, slope and time of the rising edge.

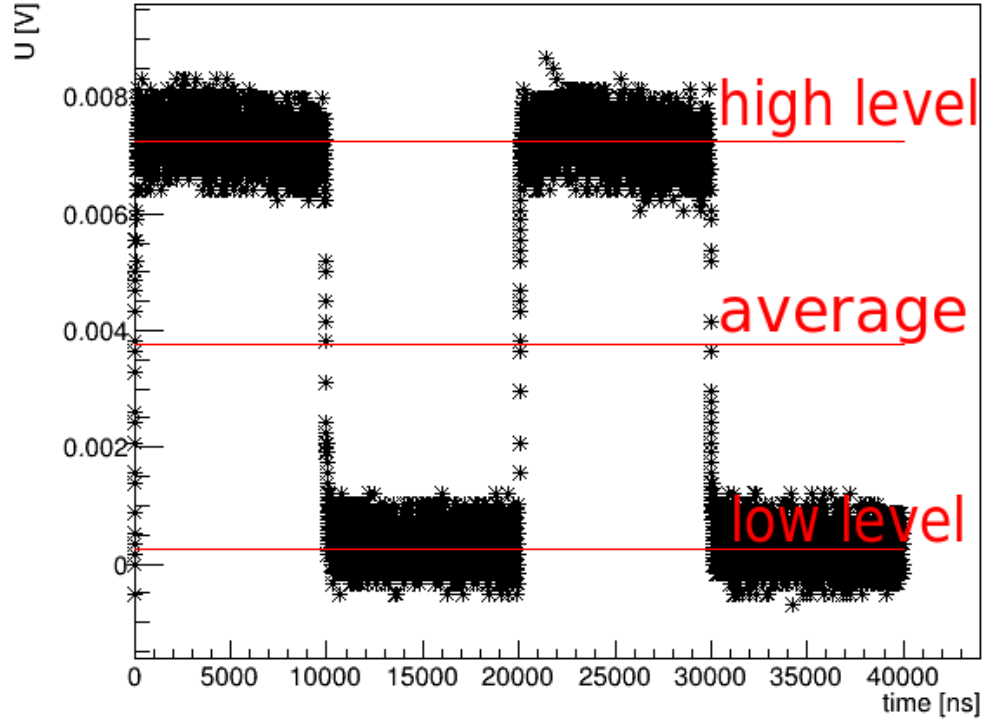


Figure 5.4: Determining the basic pulse properties - average, low and high levels of signal.

To determine the pulse height, we need to calculate the average value from all the samples at first. Then, we split the samples into two subgroups according to fact, whether they are higher or lower than the average. These subgroups are converted to histograms with fixed binning (around 5000 bins). These histograms are then fitted by gaussian. The means of these two fits determine two levels of the pulse - high ( $U_h$ ) and low ( $U_l$ ). The fig. 5.4 shows the real pulse with levels determined by this method. The height of pulse is then simply calculated by subtracting two levels:  $U_H = U_h - U_l$ .

The properties the rising edge could be specified by two parameters, which we are able to extract from our data - time and the slope of the rising edge. We are able to calculate both of them if we identify the samples, which are taken at the time of the rising. These samples' values should be between 10 % and 90 % of the  $U_H$ . First, we need to detect the rising edge in waveform data sequence. However, the signal is very noisy and this could not be simply done by detecting the exceeding of the 10 % of the  $U_H$ . To achieve that, we cycle through the waveform until we meet two conditions - the value is higher than average (and lesser than 90%) and the derivative is positive. Due to the noise, the derivative could not be calculated from two or three points, thus we use Savitzky–Golay polynom's derivative at chosen point:  $y' = \frac{1}{12h}(y_{i-2} - 8y_{i-1} + 8y_{i+1} - y_{i+2})$ . However we care only of positive/negative sign, so  $\frac{1}{12h}$ , where  $h$  is the small step, is no use for us. When these two conditions are met at some point, the program cycles back from the point through the waveform until reaches 10% level, and then beginning at the same point, which met the conditions, cycles up to reaching 90% level. All the samples traversed by this way are considered as samples of the rising edge. The rising time is calculated simply by multiplying the number of these samples

by oscilloscope's sample time (2 ns). The slope is calculated from linear fit of these samples (fig. 5.5).

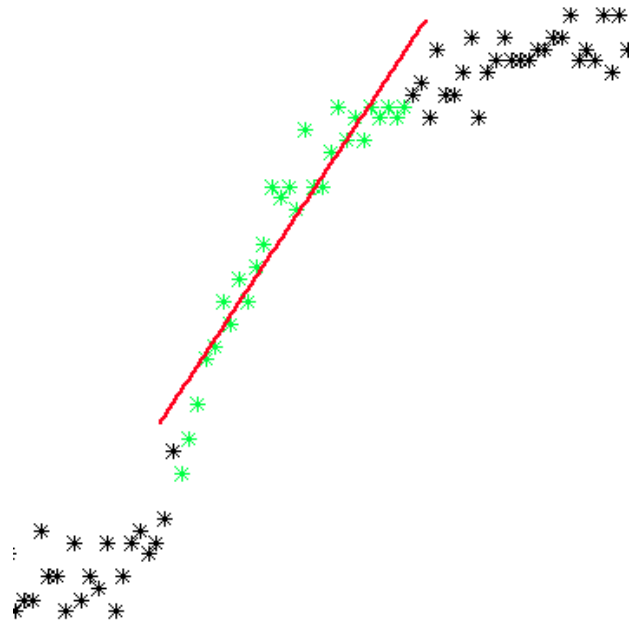


Figure 5.5: Linear fit of rising edge points (marked as green).

### 5.2.3 Results

First data taking sequence ran about two weeks. Taken data was analyzed by methods described in previous chapter and results are presented in the following graphs. The first two graphs describe optical power with respect to time (first from PM and second is the PMT pulse height).

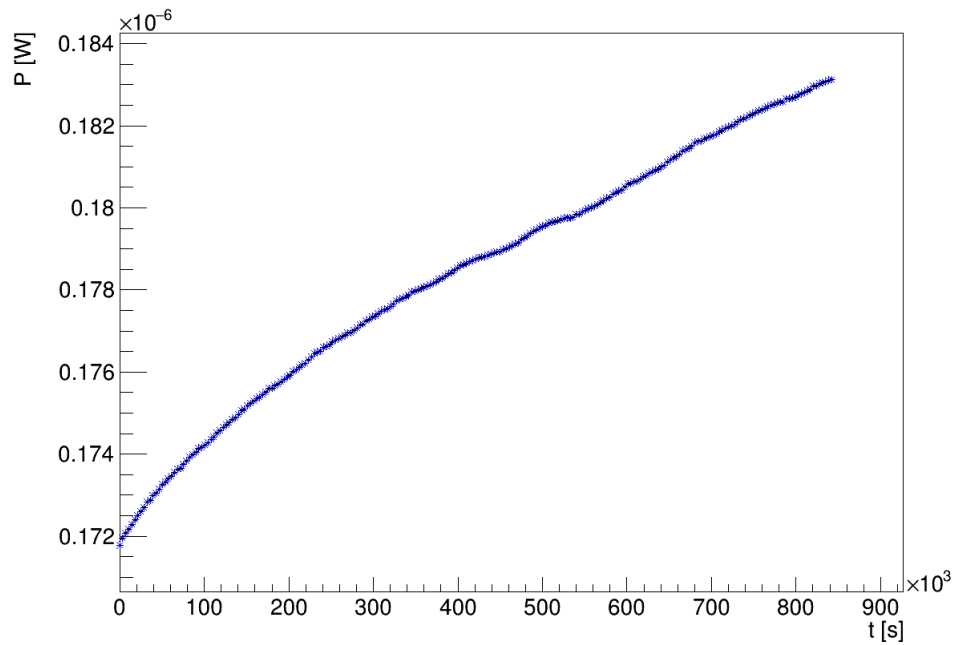


Figure 5.6: Time evolution of optical power.

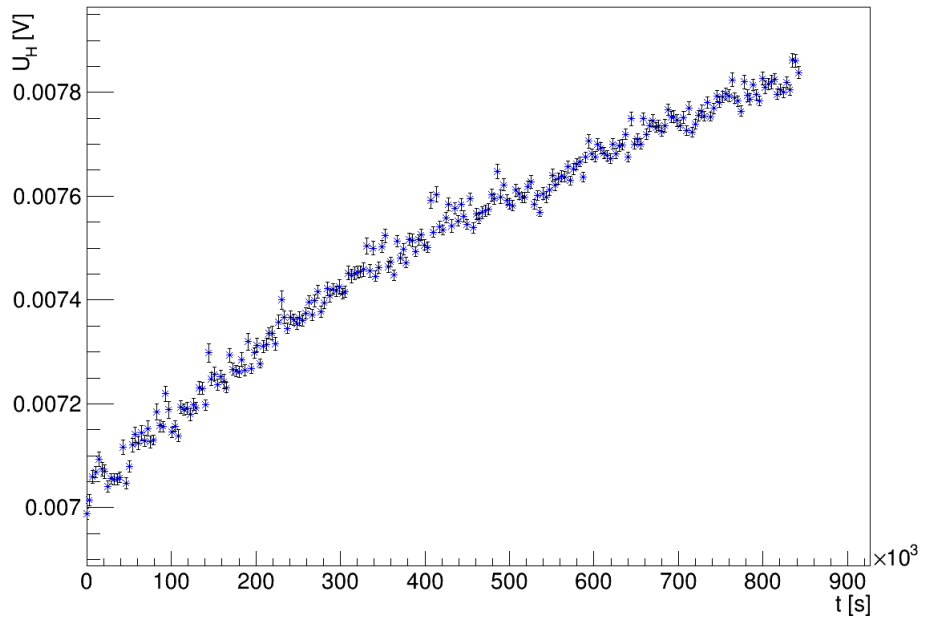


Figure 5.7: Time evolution of the pulse's height.

In the next two graphs we present calculated heights and slopes.

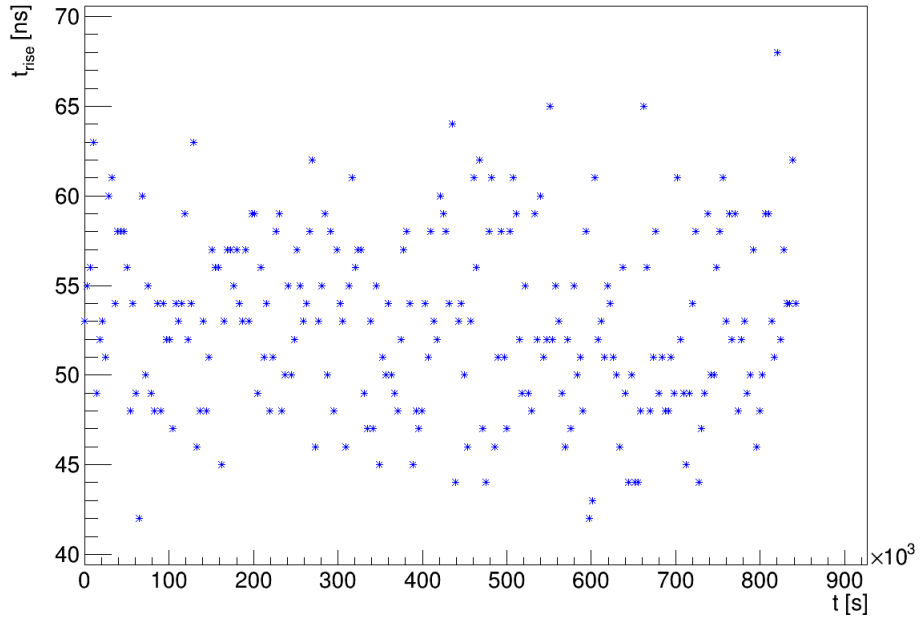


Figure 5.8: Time evolution of the pulse's edge rise time.

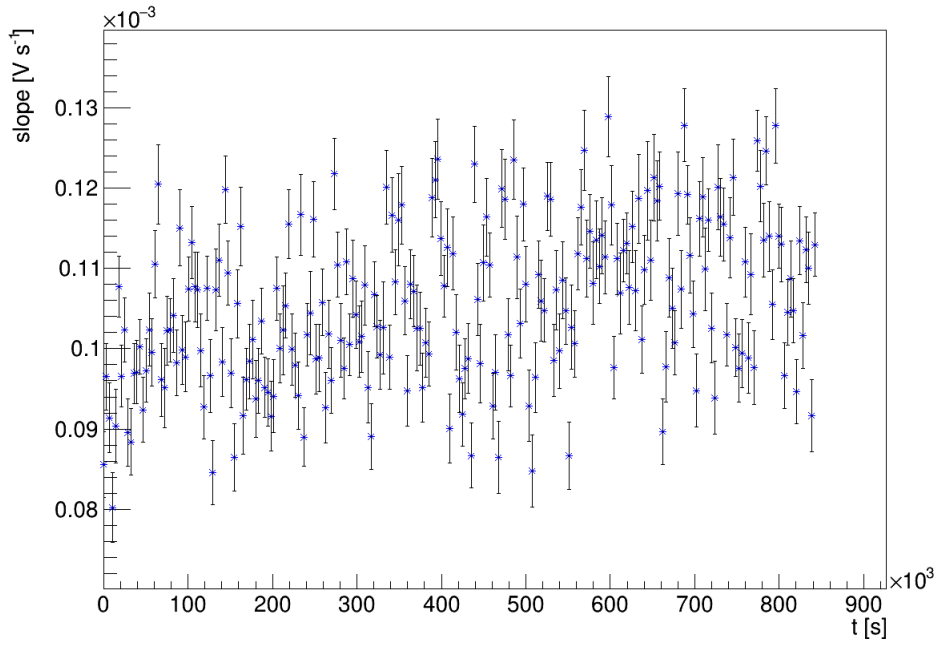


Figure 5.9: Time evolution of the pulse's edge slope.

We also measured PMT's temperature for potential gain changes.

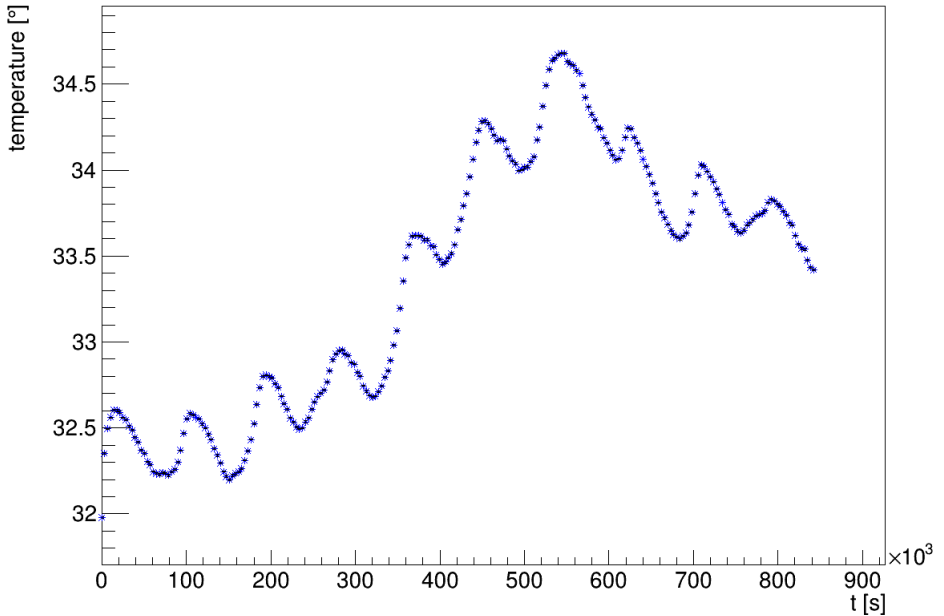


Figure 5.10: Time evolution of the PMT's temperature.

From analyzed data we may observe that the power is rising over time. This fact is confirmed by two sensors - both PM and PMT. In case of PMT there may be the drift in gain over time. Gain drift may be caused by changes in voltage (equation 4.2) or in temperature. In case of temperature, the trend is not only rising as  $U_H$ 's trend does, so the  $2^\circ$  change in temperature may play little role in  $U_H$  increase, but it is not probably the main cause of this effect. The graphs 5.8 and 5.9 shows that pulse is not deforming over time.

The optical power instability may be caused by failures in LED driving circuit (changes in current flowing by diode) or by aging processes in the UV diodes. The PM shows that the power increase is around 7% in 10 days, which is unacceptable for any calibration source.

To confirm this measured fact and check for possible causes of the optical power instability we repeated this measurement by few times with similar results. But during these measurements we used multimeter to monitor PMT's voltage. For measuring the current flowing by the diode in the internal current source circuit, we used the second channel of the oscilloscope.

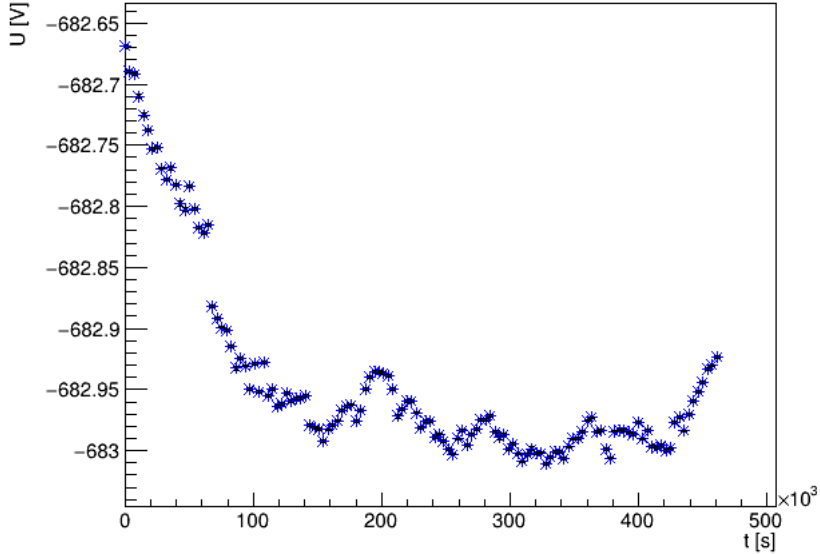


Figure 5.11: Time evolution of the PMT's voltage.

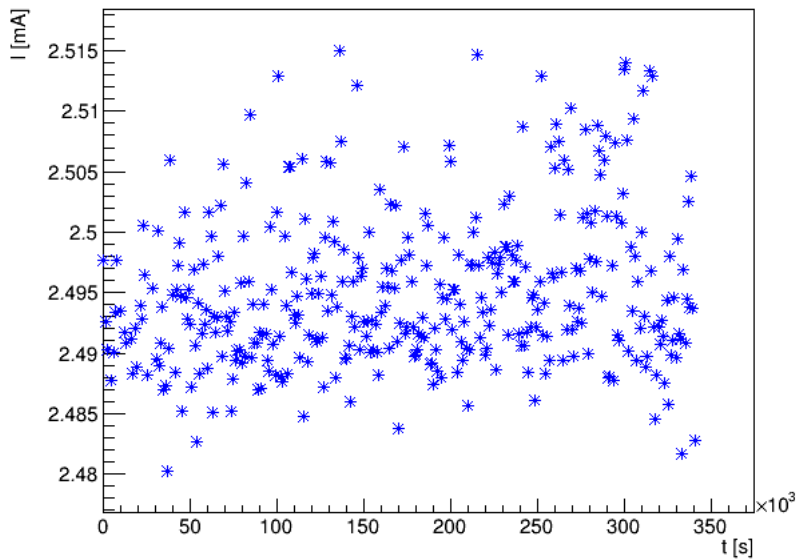


Figure 5.12: Time evolution of the UV LED's current.

Other measurements of optical power have ended in similar way. But by using the multimeter we can see that PMT's voltage is stable (fig. 5.11). It is varyiing only about 0.4 V at the beginning.

The measurement of current by oscilloscope was done and analyzed in similar way as was done for the PMT's pulses. Both of them are PWM square pulses by shape. The oscilloscope's probe was connected to the  $100\Omega$  resistor, which is in serial to the LED and the current source and acted as a simple  $U/I$  converter. As we can see in fig. 5.12, the current varies only a little over the value which was set ( $I_d = 2.5$  mA), and thus the rising trend of optical power is definitely not caused by the current variations.

## 5.3 UV LED diode aging

As was seen in results of previous measurements, the diode aging process is the most probable cause of the changes in optical power. We tried to confirm this fact by aging the similar UV LED.

## 5.4 Optical feedback - potential fix

One way to handle the aging process of UV LED diodes is to monitor the power and according to the changes set the diode current  $I_d$ . To achieve that, we tried to develop a prototype of optical feedback concept, which is based on detection UV photodiode.

The part of optical power is reflected from LED to photodiode. Photocurrent induced this way is converted to voltage which is read by ADC (analog-digital converter). This information is then used by the STM32 board to adjust the current level by DAC. One problem is that the optical power is delivered in pulses, and thus it is necessary to sample these pulses and determine the height.

### 5.4.1 Detection photodiode

As detection photodiode which we chose is GUVV-T10GD. It is guaranteed to be UV-A sensor with wavelength responsivity from 230 to 395 nm. However, it is necessary to test more of its properties, because some of the properties, which are essential for our application, are not shown in datasheets and probably haven't been yet measured - temperature dependency of the dark current, responsivity to  $10\mu\text{s}$  square signals and aging processes. The reverse voltage of photodiode  $U_r$  could go up to 2 V. With higher the  $U_r$  is, the lower is the diode's capacity.

#### Dark current

Information of dark current is very important. We need to know if the signal levels are much greater than dark current. We measured dark current with 7 set temperatures. Current was measured by keithley 2470 picoammeter. Temperature was set by autoregulated tranzistor heating plate. The tranzistor plate is driven by STM32 nucleo's DAC. The nucleo is controlled by the RPi. The RPi also communicates with picoammeter and controls the entire data acquisition. We measured two series - one with reverse voltage  $U_r = 0.1$  V and second with reverse voltage  $U_r = 1$  V. The picoammeter is also capable of adjusting voltage, so it was used as a source of reverse voltage.

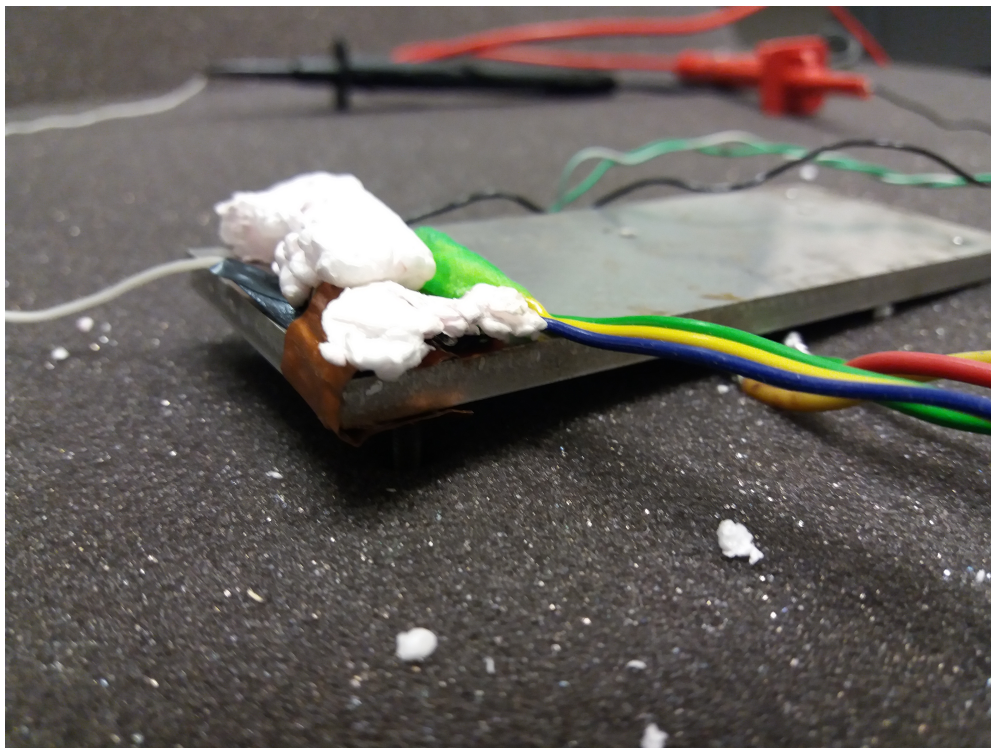


Figure 5.13: UV detection diode mounted on heating plate, covered by insulating material. The thermometer is mounted next to it.

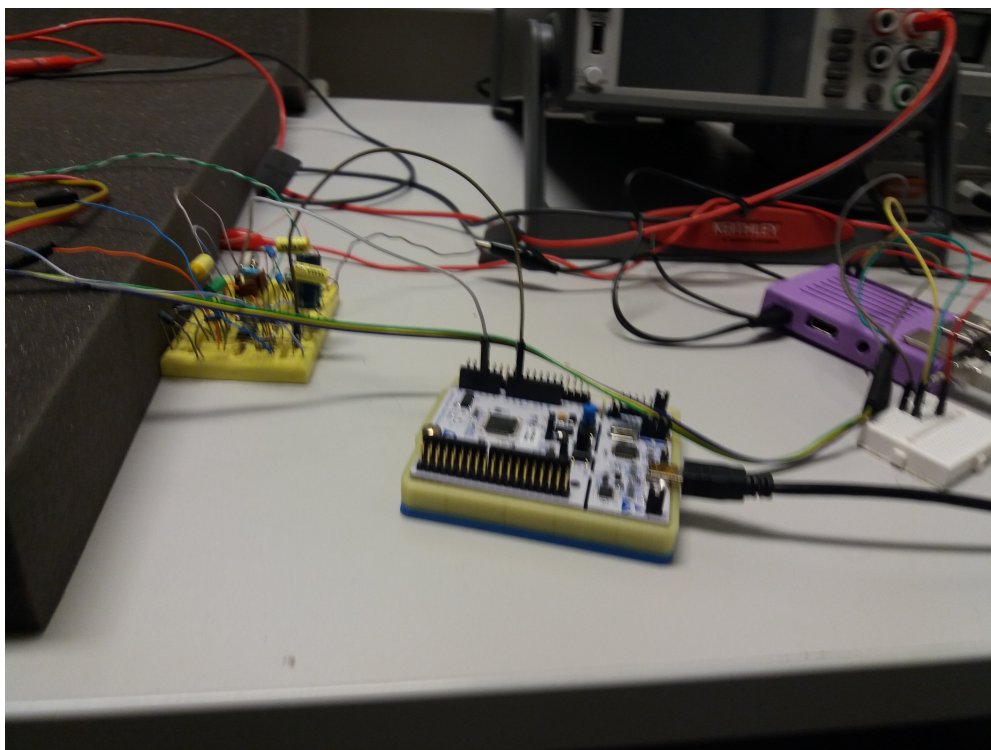


Figure 5.14: Heating control and measurement control. From the left - heating circuit, STM32 nucleo, RPi

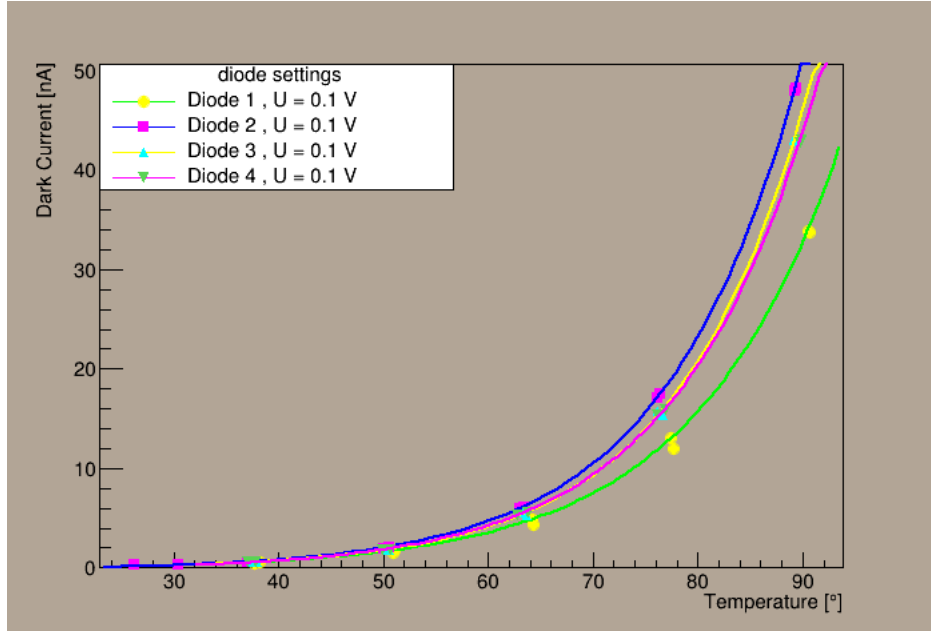


Figure 5.15: Dark currents with the reverse voltage  $U_r = 0.1$  V.

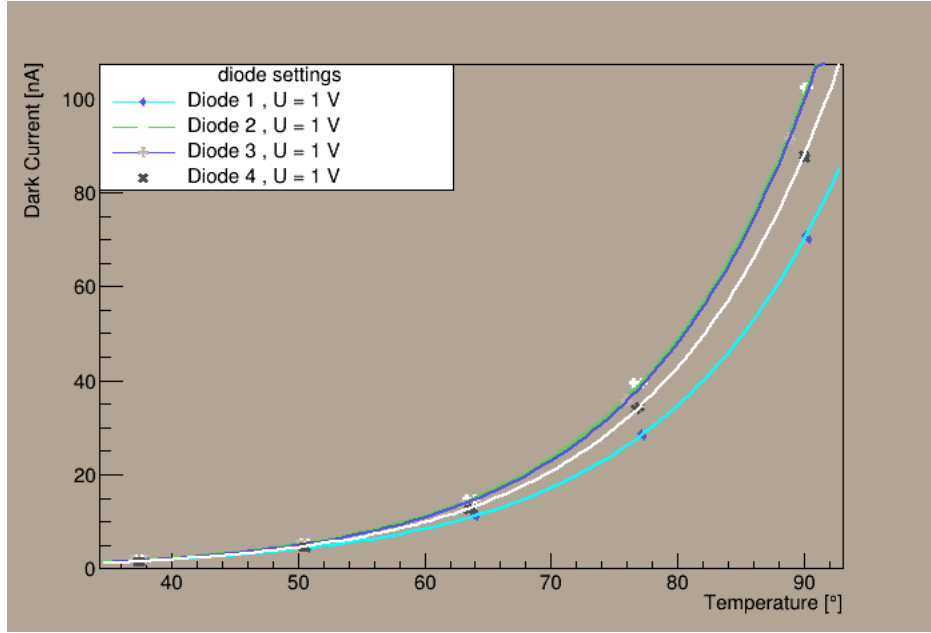


Figure 5.16: Dark currents with the reverse voltage  $U_r = 1$  V.

We measured 5 diodes. However, the dark currents of one diode were on abnormal level, and that's why its characteristics are not plot in graphs with others. This diode was not suitable for our application.

From the measured data we can see, that for the expected operating temperatures ( $t < 50^\circ$ ), the dark current is  $I_{dark} < 10$  nA.

### Signal responsivity

By direct illumination of the photodiode by the UV LED ( $I_d = 7.5$  mA) we are able to induce photocurrent about  $I_p = 5 \mu\text{A}$ , which is of the higher order than the measured dark current.

To test responsibility of the square pulses, we integrated the photodiode into the  $I/U$  transimpedance amplifier with the op-amp ADA4805 with feedback parameters  $R_F = 100 \text{ k}\Omega$  and  $C = 9 \text{ pF}$ . We illuminated the photodiode by the UV LED connected to the square pulse generator. The response could be seen on fig. 5.17.

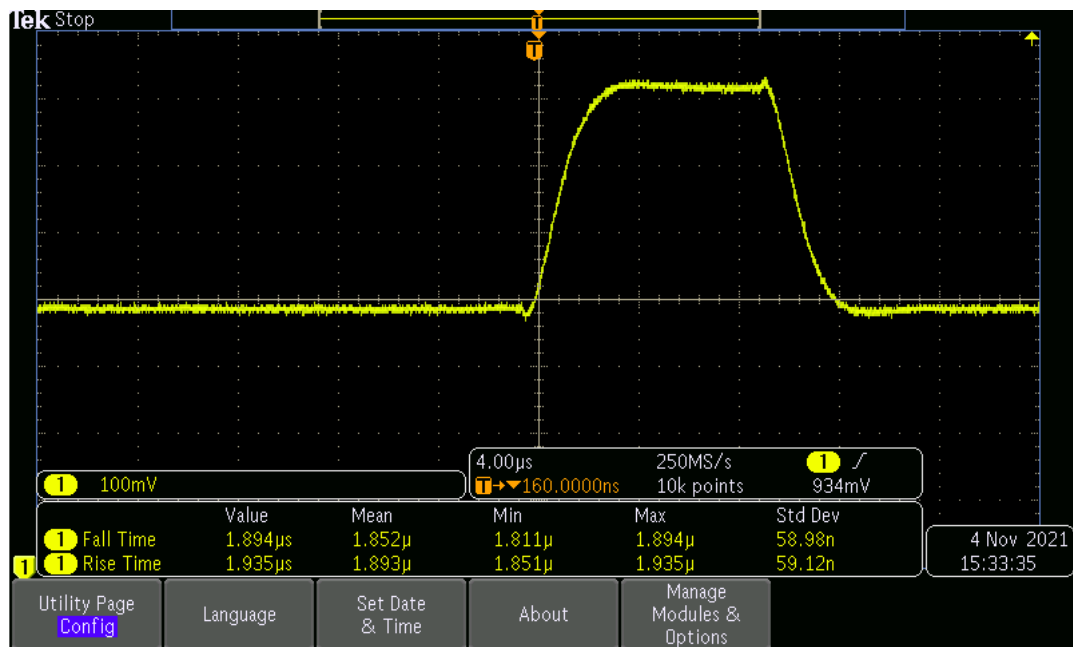


Figure 5.17: Photodiode's response on  $10 \mu\text{s}$  square pulse.

This way we are able to see the pulsing UV LED light. However, the rising edge of feedback pulse is deformed.

### Artificial aging

## 5.5 Modified UV source for drone mounting

# Chapter 6

## Monitoring system

As was mentioned before, the quality of the fluorescence detection depends on atmospheric conditions and a durability of detection parts is also dependent on exposure to these effects. Thus it is highly advised to monitor them and plan shifts according to these conditions. To capture atmospheric data, we constructed a monitoring system - a meteostation, which we describe in this chapter.

### 6.1 Monitoring of multiple FAST telescopes

The main goal was to develop a monitoring system for multiple FAST telescopes, which is capable of acquiring data of temperature, humidity, wind speed and direction, raining and light exposure. These data have to be easily accessible, so it is necessary to store them in some database, which could be accessed throughout the network.

The data could be used by operator when controlling the telescope or later in a complex analysis of detection events and calibration measurements. For example, the operator must be sure that there is no light source outside before he executes command to open the shutter of the telescope's hut. To obtain this information, he checks for the measured value from an ambient light sensor, which is a part of monitoring system.

### 6.2 Control units and sensors

Central control unit is a RPi, which collects data from other STM32 nucleos. For every FAST telescope there is one STM32 nucleo equipped with sensors (fig. 6.1), which is connected to the RPi via CAN bus. The operation scheme could be seen on (fig. 6.2). The RPi itself takes care of ultrasonic wind sensor and a rain sensor, because both wind and rain are same for every telescope. The Nucleos have connected dallas DS18B20 thermometers (1-Wire), BME230 temperature, humidity and pressure sensor(I2C) and an ambient light sensor through an optoclick module. Additional possibility is also to include induction sensor catch failures in shutter opening/closing.



Figure 6.1: STM32 with sensors.



Figure 6.2: Operation scheme of monitoring system.



Figure 6.3: Central RPi with rain and ultrasonic sensors.

### 6.3 Software system

For this application, where there is not essential to achieve fast sampling and do some fast responses, we decided to use python for RPi and micropython for STM32 nucleo. These languages offer us libraries and easy programming for some of our sensors, however in a cost of speed and memory (compared to C/C++ for example).

The data reading scripts are scheduled by classical linux's tool - crontab.

The main part of software communication between RPi (and RPi's internal processes) and Stm32 nucleos is done through the MQTT Mosquitto server, which runs on RPi. Nowadays the MQTT is a useful service used in automatization processes, where the many messages from various devices are sent and received simultaneously. The Processes could have three roles - publisher, subscriber and broker (in our case done by MQTT itself). The publisher process sends data packet with theme to broker. The broker calls all subscribers of this theme and passes them the data packet [**MqttServ**]. The processes must be programmed to communicate with MQTT service, which could be done by using various MQTT libraries. The MQTT scheme could be in our case specified in following way: The running scripts (representing processes for MQTT) for data acquisition (Wind, rain, nucleo data transfer) are programmed as publishers and

publish values of specified sensors with theme related to their names and types in specified intervals. The script, which handles the data transfer to database is programmed as subscriber.

The data are in specified intervals picked up from MQTT, and transferred into a MySQL database. The MySQL database is a part of RPi's MySQL server, and thus the data could be easily read by any other device in internal network. This database data could be also used for some web browser application to visualize the time development of local weather conditions.

Usage of this scheme, where the processes are separated and executed in scheduled times by operating system makes the system tolerant for many faults (both sensors' and nucleos' HW and SW failures) and eases the potential future upgrades.

# Chapter 7

## FAST Calibration data analysis

7.1 Photomultiplier relative calibration

7.2

7.3

# Conclusion

We are completely f\*\*\*d.

# Bibliography

- <sup>1</sup>L. Tománková, “Optical properties and calibration of the pierre auger fluorescence detector”, PhD thesis (Karlsruher Institut für Technologie (KIT), 2016), 208 pp.
- <sup>2</sup>A. Haungs, D. Kang, S. Schoo, D. Wochele, J. Wochele, W. Apel, J. Arteaga-Velázquez, K. Bekk, M. Bertaina, J. Blümer, H. Bozdog, I. Brancus, E. C. Cantoni, A. Chiavassa, F. Cossavella, K. Daumiller, V. Souza, F. Di Pierro, P. Doll, and J. Zabierowski, “The kascade cosmic-ray data centre kcde: granting open access to astroparticle physics research data”, (2018).
- <sup>3</sup>M. Malacari, J. Farmer, T. Fujii, J. Albury, J. Bellido, L. Chytka, P. Hamal, P. Horvath, M. Hrabovský, D. Mandat, J. Matthews, L. Nozka, M. Palatka, M. Pech, P. Privitera, P. Schovánek, R. Šmíd, S. Thomas, and P. Travnicek, “The first full-scale prototypes of the fluorescence detector array of single-pixel telescopes”, Astroparticle Physics **119**, 102430 (2020).
- <sup>4</sup>M. Vacula, P. Horvath, L. Chytka, K. Daumiller, R. Engel, M. Hrabovsky, D. Mandat, H.-J. Mathes, S. Michal, M. Palatka, M. Pech, C. M. Schäfer, and P. Schovanek, “Use of a general purpose integrating sphere as a low intensity near-uv extended uniform light source”, Optik **242**, 167169 (2021).
- <sup>5</sup>*Hamamatsu: photomultiplier tubes basics and applications*, [https://www.hamamatsu.com/resources/pdf/etd/PMT\\_handbook\\_v3aE.pdf](https://www.hamamatsu.com/resources/pdf/etd/PMT_handbook_v3aE.pdf).
- <sup>6</sup>S. Kliewer, *The compact cosmic ray telescope aboard the kuiper airborne observatory*, <https://cosmic.lbl.gov/SKliewer/Index.htm>.
- <sup>7</sup>*Photonis: photomultiplier tube basics*, [https://psec.uchicago.edu/library/photomultipliers/Photonis\\_PMT\\_basics.pdf](https://psec.uchicago.edu/library/photomultipliers/Photonis_PMT_basics.pdf).
- <sup>8</sup>C. RNDr. Pavel Kolář, *Z velmi vzdálených galaxií*, Czech, <https://www.fzu.cz/aktuality/z-velmi-vzdalenych-galaxii>.
- <sup>9</sup>B. Skuse, *The riddle of ultrahigh-energy cosmic rays*, <https://physicsworld.com/a/the-riddle-of-ultrahigh-energy-cosmic-rays/>.
- <sup>10</sup>P. Technology, *Picoscope ® 2000 series (a api) pc oscilloscopes and msos programmer’s guide*, <https://www.picotech.com/download/manuals/picoscope-2000-series-a-api-programmers-guide.pdf>.

Preferované jsou citace podle norem ČSN ISO 690 a ISO 690-2, popř. styly APS (American Physical Society – u prací zaměřených fyzikálně) nebo APA (American Psychological Association – u prací zaměřených více didakticky a pedagogicky).